Computers and Electronics in Agriculture 191 (2021) 106553

Contents lists available at ScienceDirect

Computers and Electronics in Agriculture

journal homepage: www.elsevier.com/locate/compag

A photogrammetry-based methodology to obtain accurate digital ground-truth of leafless fruit trees

Bernat Lavaquiol *, Ricardo Sanz, Jordi Llorens, Jaume Arnó, Alexandre Escolà *

Research Group in AgroICT & Precision Agriculture, Department of Agricultural and Forest Engineering, Universitat de Lleida (UdL) / Agrotecnio-CERCA Centre, Lleida, 25198 Catalonia, Spain

ARTICLE INFO

Keywords:
Photogrammetry
Ground-truth
Precision agriculture
3D sensors
Image-based point cloud

ABSTRACT

In recent decades, a considerable number of sensors have been developed to obtain 3D point clouds that have great potential in optimizing management in agriculture through the application of precision agriculture techniques. In order to use the data provided by these sensors, it is essential to know their measurement error. In this paper, a methodology is presented for obtaining a 3D point cloud of a central axis training system defoliated fruit tree (*Malus domestica* Bork.) obtained from stereophotogrammetry techniques based on structure-from-motion (SfM) and multi-view stereo-photogrammetry (MVS). The point cloud was made from a set of 288 photographs of the scene including the ground truth tree which was used to generate the digital 3D model. The resulting point cloud was validated and proven to faithfully represent reality. The bias of the resulting model is −0.15 mm and 0.05 mm, for diameters and lengths, respectively. In addition, the presented methodology allows small changes in the ground truth actual tree to be detected as a consequence of the wood dehydration process. Having an actual and a digital ground-truth is the basis for validating other sensing systems for 3D vegetation characterization which can be used to obtain data to make more informed management decisions.

1. Introduction

According to the official ISPA definition, *Precision agriculture (PA) is a management strategy that gathers, processes and analyzes temporal, spatial and individual data and combines it with other information to support management decisions according to estimated variability for improved resource use efficiency, productivity, quality, profitability and sustainability of agricultural production* (International Society for Precision Agriculture (ISPA), n.d.). Therefore, PA is able to improve the profitability and sustainability of the agricultural production and optimizes the use of available resources. Considering the need to produce food to feed a growing population while reducing the impact of agriculture on the environment at the same time, PA is a good strategy to achieve these goals (Gené-Mola et al., 2020; Rosell-Polo et al., 2015; Talebpour et al., 2015).

The study of the plant geometry (i.e. size, volume, shape) and structure (i.e. leaf density, leaf area index, canopy porosity, woody structure and training system) is essential since it is related to fundamental properties and environmental interactions of plants (Arnó et al., 2013; Méndez et al., 2013). Therefore, from the study of the geometry of the tree it is possible to estimate the long-term productivity, the yield production, the tree biomass and the water consumption (Lee & Ehsani, 2009). Before the advent of the first 3D characterization sensors, it was very laborious, even, impossible to realize an accurate commercial scale 3D crop characterization. Nowadays, there are sensing systems which allow 3D canopy characterization to be performed in a relatively simple and fast way. However, it should be noted that 3D scanning presents some non-minor difficulties: (i) the high number of elements, (ii) the arrangement in space makes it, from any point of view, have elements partially or totally in hidden areas and (iii) the high geometric complexity, with all kinds of diameters and angles, of the trees architecture (Sanz-Cortiella et al., 2011).

The principal 3D techniques applied in agriculture are digital photogrammetric techniques, linear array of light sensors, stereo vision and LiDAR sensors (Rosell & Sanz, 2012). These technologies are interesting as they are non-destructive, allowing the monitoring over time to be implemented (Paulus, 2019).

Vegetation characterization technologies would allow changes in tree structure to be quantified at different moments during the season and use the results to improve the management of agricultural resources and orchard operations (plant protection product applications, fertilization, irrigation, etc.), reducing economic and environmental costs

* Corresponding authors.
E-mail addresses: bernat.lavaquiol@udl.cat (B. Lavaquiol), alex.escola@udl.cat (A. Escolà).

https://doi.org/10.1016/j.compag.2021.106553
Received 9 June 2021; Received in revised form 26 October 2021; Accepted 5 November 2021
0168-1699/© 2021 The Authors. Published by Elsevier B.V. This is an open access article under the CC BY-NC-ND license (http://creativecommons.org/licenses/by-nc-nd/4.0/).

(Rosell & Sanz, 2012). It could also make the detection and classification of tree organs possible and that may be of interest in the decision-making process to optimize operations in fructiculture/horticulture (Rosell-Polo et al., 2015).

Images have the potential to provide very accurate 3D information at different scales. Photogrammetry techniques allow 2D and 3D metric information to be extracted from digital images (Forlani et al., 2015). In the recent years, a number of software packages (e.g. Agisoft PhotoScan or Agisoft Metashape, DroneDeploy, Pix4Dmapper Pro) have emerged and are capable of using RGB images to create 3D point clouds (Walter et al., 2018). In addition, advances in photogrammetry are closely linked to improvements in computer vision. Since computer vision is a mainstream topic, photogrammetry is expected to continue to evolve and improve (Forlani et al., 2015; Goodbody et al., 2021). One of the strengths of photogrammetry is that produces very detailed 3D models and provides surface color information (An et al., 2017). From its beginning, the main application of photogrammetry has been the creation of maps, but it is being used successfully in fields such as industrial metrology, architecture, medical and forensic imaging among many others (Forlani et al., 2015; González-Jorge et al., 2012).

Recently, photogrammetric techniques are also used in agriculture. Research works have applied photogrammetry to accurately estimate the grassland yield (Grüner et al., 2019), to obtain the external surface of tomato plants (Aguilar, 2007), for apple detection and 3D location (Gené-Mola et al., 2020), to measure leaf length and rosette area (An et al., 2017) and to disclose canopy architecture in olive trees (Moriondo et al., 2016). Miller et al. (2015) tested the ability of structure-from-motion (SfM) together with multi-view stereo-photogrammetry (MVS) to create accurate 3D point cloud models from which volume and linear tree metrics can be estimated. Regarding applications in forest science, Liu et al. (2018), designed a low-cost continuous terrestrial photogrammetry-based system with real-time kinematic (RTK) correction to obtain georeferenced forest accurate point clouds and Liang et al. (2014) estimated the diameter-at-breast-height (DBH) from a point cloud generated with an uncalibrated hand-held camera.

When 3D scanning techniques are used, it is necessary to be aware about the measurement error. Palacin et al., (2008) and Palleja et al. (2010) determined that the tree volume measurement error from a terrestrial LiDAR scanner was less than 6 % and 4.4 %, respectively.

Escolà et al., (2017) measured the canopy volume of an intensive olive commercial grove with a LiDAR-based system and observed that the results coincided with measurements obtained with conventional manual techniques used in fruticulture. However, the authors questioned whether those measurements obtained with conventional techniques are valid as ground-truth (GT) when comparing them to higher resolution measurements, such as those obtained with LiDAR-based systems. The authors expressed the need for high-resolution and high accuracy measurements to be used as ground-truth. Yang et al., (2019) also denote the lack of ground-truth when studying the influence of vegetation characteristics on individual tree segmentation methods with LiDAR-derived data.

In view of this background, the objective of the present work is to create a methodology to obtain a digital 3D replica of an actual defoliated tree using RGB images and stereo-photogrammetry techniques based on Structure from Motion (SfM) and Multi-View Stereo (MVS) (Jin et al., 2005; Westoby et al., 2012) and subsequently validate it by measuring and comparing diameters and lengths with the actual tree ground-truth. As it seeks to create a replica as accurate as possible, the images were acquired in optimal conditions (indoors, with controlled light and background and without movement of the branches by the wind). This replica could be used as a digital ground-truth to validate other scanning systems and technologies in field conditions by assessing the accuracy of the obtained 3D point clouds comparing them with the accurate digital replica.

2. Material and methods

2.1. Ground-truth selection

The actual fruit tree used as a reference or ground-truth (GT) was an apple tree (*Malus domestica* Bork.) planted with a central axis training system. That training system was chosen as it is one of the most common in the region of Lleida, Catalonia. The fruit tree was cut down, defoliated and fixed on a wood pallet on wheels in 2015. The height of the fruit tree was 2.5 m and the maximum width 2 m. Hereafter, that actual tree will be referred to as ground-truth (GT). The GT is preserved as a whole in the laboratory.

2.2. Digital ground-truth generation

To create a 3D digital version of the GT, hereafter the digital ground-truth (DGT), stereo-photogrammetric techniques based on Structure from Motion (SfM) and Multi-View Stereo (MVS) were applied to an image data set of the GT.

Usually, when a photogrammetric model is generated, the object is fixed in a central position and the camera moves around taking photographs from different angles. Later on, a computer program processes the images looking for matches between pairs of photographs and computes the position of the camera for each shot using SfM. Finally, the distance to the camera of each pixel in an image is determined by MVS and placed in a three-dimensional space. This way, when all the common points of all the images are joined, a dense 3D point cloud of the scene is obtained. However, in order to control the lighting conditions, in this study it was decided to take pictures inside a building and, due to the lack of space, the camera remained fixed, and the GT was rotated around its vertical axis, so that a picture was taken every 10° rotation of the GT. A white background was installed behind the GT.

The photographs were taken with a camera EOS-60D 18 MP CMOS Digital SLR (Single Lens Reflex) (Canon, Tokyo, Japan) equipped with EF 50 mm f/1.4 lens (Canon, Tokyo, Japan). It was decided to work without zoom in order to facilitate the detection of common points in the different photographs. The photographs were taken with f / 22 diaphragm aperture, which is considerably closed to provide a depth of field large enough to include the whole scene. The shutter speed ranged from 2 s to 3.2 s. Although the data acquisition was done indoor, the shutter speed varied as the lighting conditions varied during the trial depending on the position of the sun entering through the windows. That range of shutter speeds allowed all the details of the GT to be distinguished optimally, even the finest branches, and to capture the colors correctly. The white balance of the camera was 6000 K and the sensor sensitivity was set to ISO100.

The camera was 4 m away from the trunk of the GT and the photographs were taken decentered from 0.4 m to the left of the GT horizontal axis (Point A in Fig. 1) and then from 0.4 m to the right (Point B in Fig. 1). Those two positions, right and left, were decided in order to generate stereoscopy and because the width of the GT could not fit into a single photograph from 4 m of distance (Fig. 1). The photographs were taken at 4 heights (0.77 m, 1.33 m, 1.89 m and 2.45 m). The total number of photographs taken was 288, corresponding to 36 photographs (one every 10° rotation of the GT) from each position (A and B) and 4 heights.

The program used to process the images and obtain the 3D DGT point cloud was PhotoScan Professional 1.1.6 (Agisoft LLC, St. Petersburg, Russia). This program is based on SfM and on MVS (Koci et al., 2017), operates with arbitrary images and performs well both when images are taken under controlled lighting conditions or when taken in uncontrolled environments. In order to be able to carry out the reconstruction it is necessary to have at least two different views of the object. The alignment of the images and the generation of the 3D model are fully automated.

In a first attempt, the output of the process was not satisfactory. That

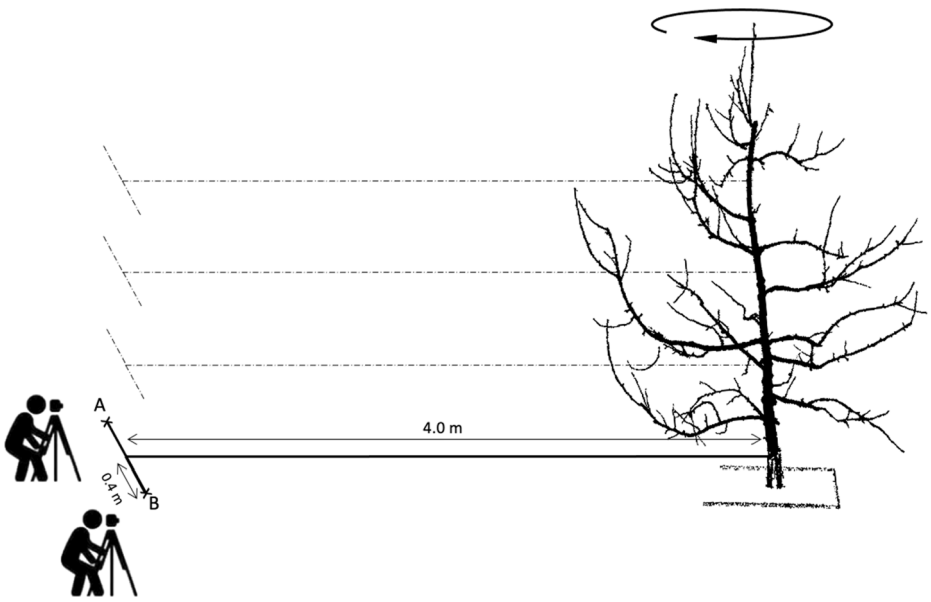

Fig. 1. Outline planar view of the positions from where the photographs were taken.

was attributed to the white plastic background creases and shadows which made it not perfectly solid. To avoid that problem, the background of the scene was removed from all the 288 images using Photoshop® CS3 extended v10.0 (Adobe Systems Incorporated, San Jose, CA). This was done with an automatic process in which an alpha channel (mask) was created to identify the background of all the images. PhotoScan uses the three RGB channels and the alpha channel to apply the reconstruction. The pixels marked in the alpha channel were ignored during the 3D modelling process. PhotoScan was used to match them, and the 3D replica was generated. To make the program work better, the images were joined together by height chunks. That is, the images of the same height were joined first and then all heights were computed to create a single cloud.

When a 3D replica is created, the program does not know the distance at which the images are taken so the tree 3D replica has incorrect dimensions. To solve this problem, the model needs to be scaled. To scale the 3D replica, the distances between 11 points of the GT were measured and entered into the 3D model. Those points were selected along all direction and heights, so that digital scaling is true to reality without distortions.

The final result was a DGT, with relative coordinates (x,y,z) for each point. The cloud obtained was composed of 49,751,573 points. Because the number of points was high the computer resource demand was also high. For a more convenient DGT manipulation, a random subsampling of the cloud was performed to obtain a 1-million-point cloud. That operation was performed in the program CloudCompare v2.6.1 (EDF R&D, París, France). The resulting point cloud had an average distance between points of 0.6 mm. Each point, in addition to its relative coordinates x, y and z, included RGB data of the assigned display color.

2.3. Digital ground-truth validation

In order to validate the DGT, a number of corresponding trunk and branch diameters and lengths were measured both on the GT and the DGT (Fig. 2). The diameters where selected taking into account to be evenly distributed over the range of diameters present in the GT. Few

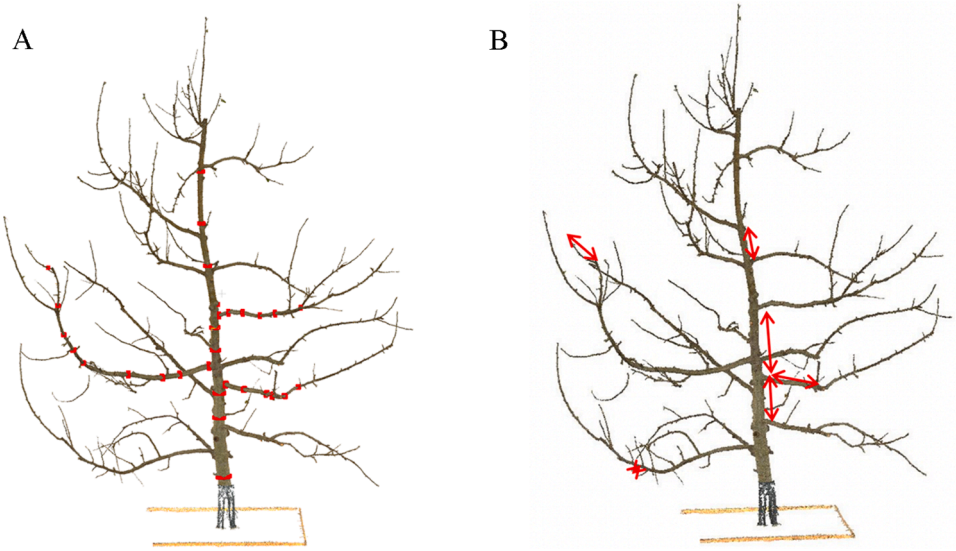

Fig. 2. 3D view of the digital ground-truth (DGT) with the location of the measured diameters (A) in red and the measured lengths (B) with red arrows measured on the ground-truth (GT) and DGT. (For interpretation of the references to color in this figure legend, the reader is referred to the web version of this article.)

trunk diameters were measured from the base to the end of some main branches. In order to ensure the presence of all diametric classes, several branches were selected. Measurements were made with a calliper on the GT and with the measuring tool "point picking" of CloudCompare on the DGT. In both the GT and the DGT, 4 measurements of each diameter were made in 4 different directions at each selected point, and the average was computed to provide a diameter value as close as possible to the actual one. To obtain the diameters on the DGT, a thin slice of the point cloud was selected from the section of the tree to be measured using CloudCompare. Then, the diameter was obtained following the aforementioned method based on 4 measurements.

Descriptive statistics were applied on the absolute error (Equation (1)) presented by the paired data of the DGT with respect to the GT. The accuracy of DGT was also evaluated using the bias (Equation (2)), the standard deviation (Equation (3)) and the root mean square error (RMSE) (Equation (4)).

$$\overline{\varepsilon_a} = \frac{\sum_{i=1}^{n} \left| y_i - \widehat{y}_i \right|}{n} \tag{1}$$

$$Bias = \frac{\sum_{i=1}^{n} \left(y_i - \widehat{y}_i \right)}{n} \tag{2}$$

$$\sigma = \sqrt{\frac{\sum_{i=1}^{n} (\varepsilon_{ai} - \overline{\varepsilon_a})^2}{n}} \tag{3}$$

$$RMSE = \sqrt{\frac{\sum_{i=1}^{n} {\varepsilon_{ai}}^2}{n}} \tag{4}$$

where $\widehat{y}_i$ is the i^{th} estimate (diameter or length), y_i is the i^{th} reference and n is the number of estimates. In addition, a statistical analysis of the paired data was performed which consisted of performing a simple regression analysis of the GT (y) over DGT (x). The null hypothesis is that the intercept of the regression (β_0) is 0 and the slope (β_1) is 1, that is y = x. It will be accepted that there are no significant differences between the GT and the DGT when $\beta_0 = 0$ and $\beta_1 = 1$. Given that the variables β_0 and β_1 are not independent, an inequality is posed in which β_0 and β_1 covary. So, a confidence region is constructed to allow both coefficients to be contrasted simultaneously. The 95 % confidence region for the aforementioned parameters (an elliptical shape for the two-dimensional case) is given by Equation (5),

$$n(\beta_0 - a)^2 + 2(\beta_0 - a)(\beta_1 - b)\sum x_i + (\beta_1 - b)^2 \sum x_i^2 \leq 2\widehat{\sigma}^2 F_{p,n-p}^{(\alpha)} \tag{5}$$

where n is the number of observations; β_0 is the statistical parameter of the model representing the intercept; a is the estimate of β_0 from the model fit to the sampling data; β_1 is the statistical parameter of the model representing the slope; b is the estimate of β_1 from the model fit to the sampling data; x_i are the values of the DGT; $\widehat{\sigma}^2$ is the variance estimated by the mean square error; and $F_{p,n-p}^{(\alpha)}$ is the F-value at α significance level for n and n-p d.f., being p the number of parameters of the model (in our case, $p = 2$). The question is whether this elliptical confidence region contains the point (β_0 , β_1) with coordinates $\beta_0 = 0$ and $\beta_1 = 1$. Substituting these values in Equation (5) is only a matter of checking whether the inequality is satisfied. If the confidence region includes the point $\beta_0 = 0$ and $\beta_1 = 1$, it can be said that GT and DGT present no statistically significant differences with an α significance level.

The tree was cut down and defoliated in 2015 and just after that the photographs were taken, so the DGT was generated. However, the validation of diameters and lengths was done after three years, in 2018, when the physical measurements on the GT were taken. It is expected for the tree to suffer dehydration to some extent. Spices with similar wood density as apple trees experience total radial contraction between 4 and 6 % due to dehydration (Gutiérrez & Plaza, 1967). If significant differences between GT and DGT diameters and lengths were found, the reason could be dehydration during this time interval. In that case, a new digital ground-truth (nDGT) would be generated and validated.

3. Results and discussion

The absolute errors of the diameters of the DGT with respect to the GT range from 0.18 mm to 5.03 mm with an average of 1.68 mm, a standard deviation of 1.20 mm, a bias of 1.10 mm and a RMSE of 2.06 mm (Table 1). The average relative error in DGT diameters with respect GT is 5.64 %. Fig. 3A shows the DGT and GT diameter scatter plot diagram and the adjusted linear model. It is observed that the paired diameters have a high correlation, but the adjusted linear model does not fit the y = x line (slope less than 1). The elliptical confidence region determined according to Equation (5) does not contain the point $\beta_0 = 0$ and $\beta_1 = 1$ (Fig. 9). Thus, there are significant differences between the diameters measured on the GT and on the DGT.

In addition, the absolute errors of the DGT lengths range from 0.20 mm to 5.20 mm with an average of 1.35 mm, a standard deviation of 1.94 mm, a bias of 0.92 mm and a RMSE of 2.23 mm (Table 1). It is observed that the paired lengths have a very high correlation and that, in addition, the linear model adjusted is close to the y = x line (Fig. 3B). The elliptical confidence region (Equation (5)) includes the point $\beta_0 = 0$ and $\beta_1 = 1$ (Fig. 9). Thus, there are no significant differences between GT and DGT lengths.

The significant differences between GT and DGT diameters can have several explanations. The first possibility is that the measurements were not taken correctly. The second is that the photogrammetric techniques used or the procedure followed did not allow the actual model to be reconstructed with sufficient accuracy. The third is that during the time elapsed since the digital ground-truth was generated in 2015 and its validation in 2018 the ground-truth model may have varied. After replicating some of the measurements, the first option was discarded. In relation to the third option, since the photographs to generate the DGT were taken a few days after the tree was cut down, in 2015, and the ground-truth validation manual measurements were performed three years after, it could have happened that the wood underwent a dehydration process that modified the GT diameters of the trunk and branches.

The wood shrinkage happens in radial directions (from the the periphery of the tree trunk or branches to their central axis) and varies from 2 % to 7 % (Stamm, 1935). Data on total radial contraction of different tree species were consulted, but that for *Malus* ssp. were not found. Thus, species with similar density were used as reference. *Alnus* ssp. has a total radial contraction of 4 %, *Betula* ssp. has a total radial contraction of 4.33 % and *Fagus* ssp. has a total radial contraction of 5.66 % (Gutiérrez Oliva & Plaza Pulgar, 1967). In this work, the mean DGT diameter is about 6 % larger than the GT. That is consistent with the

Table 1
Descriptive statistics results of the absolute error of diameters and lengths for each comparison: ground-truth vs digital ground-truth (GT – DGT), ground-truth vs reduced digital ground-truth (GT – rDGT) and ground-truth vs new digital ground-truth (nDGT).

	Diameters			Lengths		
	GT - DGT	GT - rDGT	GT - nDGT	GT - DGT	GT - rDGT	GT - nDGT
Mean absolute error (mm)	1.68	0.38	0.29	1.35	9.10	1.31
Bias (mm)	1.10	0.04	−0.15	0.92	−9.10	0.05
Standard Error (mm)	0.22	0.10	0.07	0.79	1.61	0.65
Standard Deviation (mm)	1.20	0.41	0.41	1.94	3.96	1.60
RMSE (mm)	2.06	0.55	0.49	2.23	9.79	1.97
N	29	17	32	6	6	6

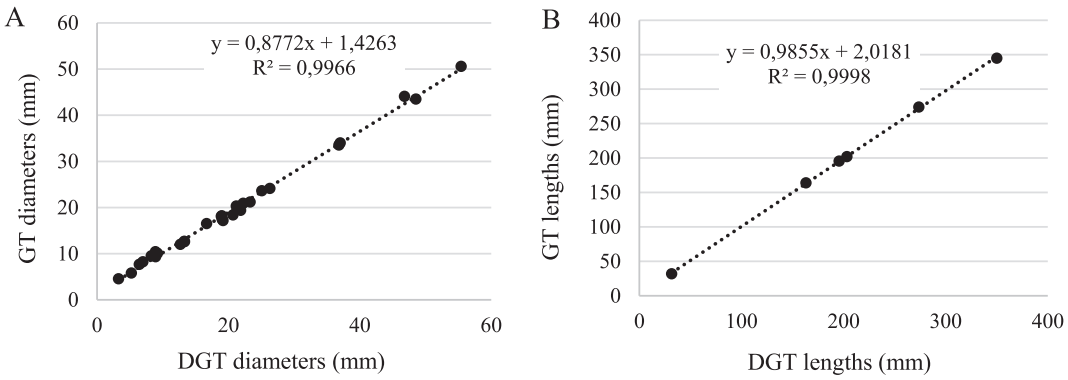

Fig. 3. Linear models adjusted between ground-truth (GT) and digital ground-truth (DGT) diameters (A) and lengths (B) including the line fit equation and the coefficient of determination.

previously cited literature. Hence, it was decided to downscale DGT to create a new point cloud 6 % contracted. Diameters and lengths were re-measured on the point cloud, and a new statistical analysis was applied. The new point cloud was named reduced digital ground-truth (rDGT).

The diameter absolute errors of the rDGT range from 0.03 mm to 1.62 mm with an average of 0.38 mm, a standard deviation of 0.41 mm, a bias of 0.04 mm and a RMSE of 0.55 mm (Table 1). Fig. 4A shows the rDGT and GT diameter scatter plot diagram and the adjusted linear model. It is observed that the paired diameters have a high correlation and that the adjusted linear model is close to the y = x lineA). Although there are statistically significant differences between diameters of the rDGT with respect to the GT, the elliptical confidence region (Equation (5)) is quite close to the point $\beta_0 = 0$ and $\beta_1 = 1$ (Fig. 9).

The absolute errors of the lengths measured on the rDGT range from 2.10 mm to 11.90 mm with an average of 9.1 mm, a standard deviation of 3.96 mm, a bias of −9.10 mm and a RMSE of 9.79 mm (Table 1). It is observed that the paired lengths have a very high correlation and that, in addition, the adjusted linear model is close to the y = x line (Fig. 4B). However, the confidence region (Equation (5)) moves away from the point $\beta_0 = 0$ and $\beta_1 = 1$ (Fig. 9). Thus, there are significant differences between GT and rDGT lengths. Thus, the rDGT, created by downscaling the original DGT by 6.0 %, accurately reproduces the diameters of the GT but, regarding lengths, significant differences are found between rDGT values and GT.

The explanation for that is that DGT was shrunk a 6 % in all three dimensions (x,y,z) in contrast, dehydration causes radial shrinkage in the trunks and branches while longitudinal shrinkage is practically negligible (Stamm, 1935). It is therefore logical that the rDGT correctly represents the diameters but misrepresents the lengths. Hence, it is to be concluded that the problem might not be the methodology to create the DGT but the process of dehydration of the GT. Since the rDGT is invalid, it was decided to create a new DGT of the same tree. That photogrammetric reconstruction was made from photographs taken in 2018, once the GT was completely dehydrated, and was build according to the same procedure described in the materials and methods section.

The resulting point cloud was named new digital ground-truth (nDGT), Fig. 8 shows the obtained point cloud with extended details. When nDGT is compared to the DGT several differences arised (Fig. 5). Fig. 5A shows the point clouds of the DGT (black) and the nDGT (green) overlapped. It is observed that the position of the branches changes significantly between the DGT and the nDGT. The differences are due to changes in the angles of insertion of the branches into the trunk or to twisting of the same branches, which causes significant displacements at the branch ends. These changes are caused by the wood dehydration. In order to quantify the differences, the CloudCompare cloud-to-cloud distance tool was employed. Fig. 5B shows the DGT point cloud colored according to the absolute error calculated relative to the nDGT. Moreover, it also clarifies the reason why those changes did not affect the lengths measured in DGT, as they were taken between point that did not suffer important relative displacements (Fig. 2B).

Bluish points in Fig. 5B represent variations between the two clouds smaller than 3 cm. It is observed that most of the points in the DGT cloud maintain its position in almost the same location as in the nDGT cloud. Greenish points represent variations between 5 cm and 10 cm. These variations occur from the middle of the branches to their ends. Yellowish points represent errors between 10 and 15 cm and orange points represent errors between 15 and 20 cm. These magnitudes are found in the last third of some of the branches. Red points represent errors between 20 and 35 cm. These errors are at the very end of a few branches.

When analyzing the results, it is observed that the absolute errors of

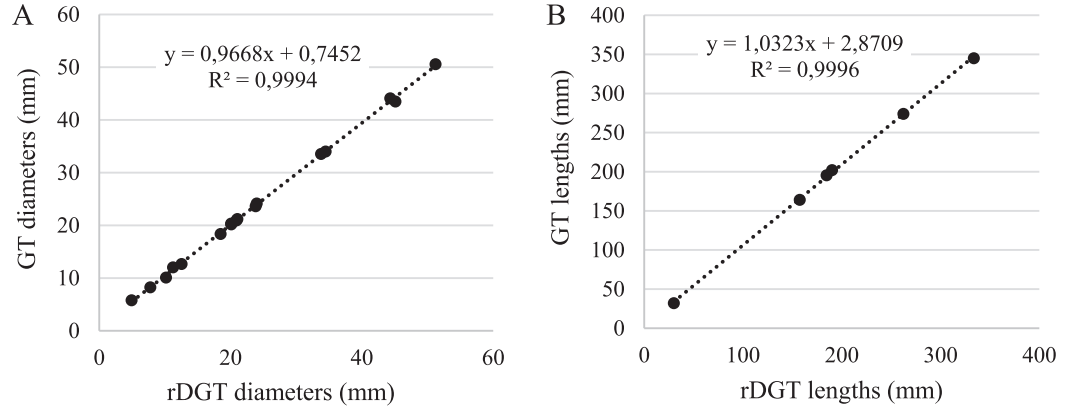

Fig. 4. Linear models adjusted between ground-truth (GT) and reduced digital ground-truth (rDGT) diameters (A) and lengths (B) including the line fit equation and the coefficient of determination.

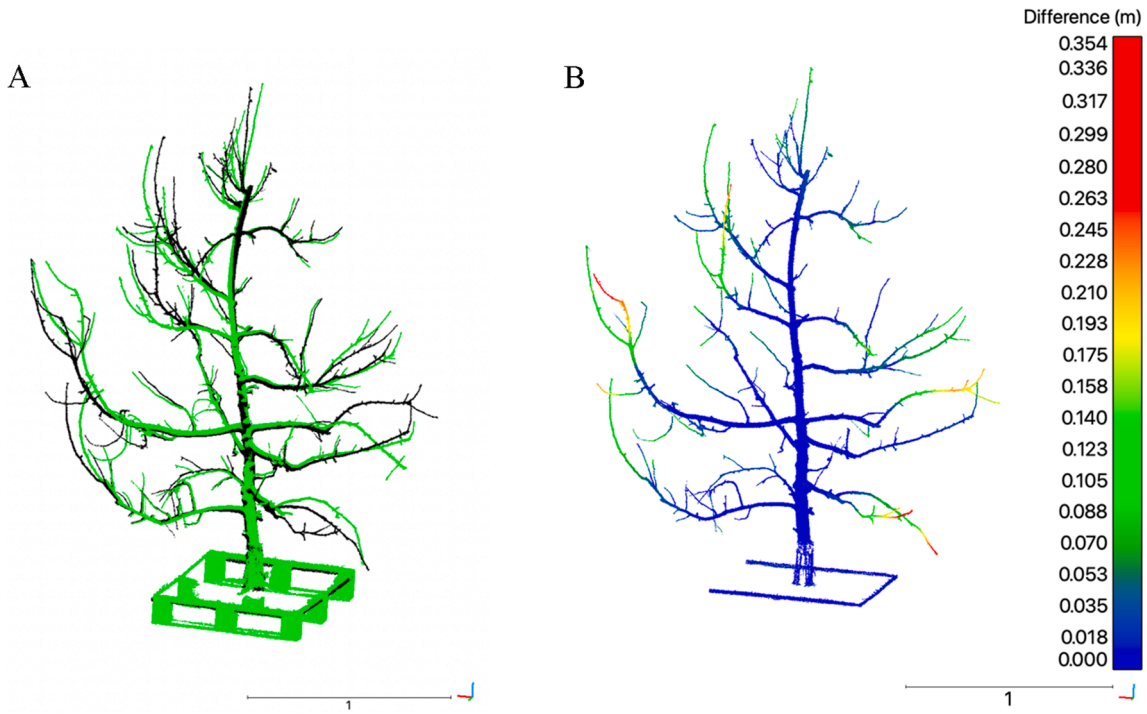

Fig. 5. Overlapping of the digital ground-truth (DGT), in black, and the new digital ground-truth (nDGT), in green, to observe the differences caused by wood dehydration (A). The DGT is colored based on the cloud-to-cloud distances (difference) to nDGT (B). (For interpretation of the references to color in this figure legend, the reader is referred to the web version of this article.)

the diameters in nDGT range from 1.90 mm to 0.02 mm with an average of 0.29 mm, a standard deviation of 0.41 mm, a bias of −0.15 mm and a RMSE of 0.49 mm (Table 1). Fig. 7A shows the nDGT and GT diameter scatter plot diagram and the adjusted linear model for diameters. It is observed that the paired diameters have a high correlation and the adjusted linear model is close to the y = x line. The elliptical confidence region (Equation (5)) is very close to the point $\beta_0 = 0$ and $\beta_1 = 1$ although is not containing it (Fig. 9). The confidence region narrowly missed the point of contrast for a significance level of 5 % when tree branch diameters were validated. The hypothesis of equality of the GT and nDGT models is also refused using a statistical significance of 1 %. Although this increased the confidence in accepting the equality of models (if this hypothesis is true), the power of the test may reach too low values due to the increase in the type II β error (or probability of accepting equality of the two models when in fact they are different). Despite decreasing the statistical significance to 1 %, it is observed that the confidence region includes $\beta_0 = 0$ but not $\beta_1 = 1$, although it is extremely close (Fig. 6).

The absolute errors in the lengths measured on the nDGT range from 4.00 mm to 0.00 mm with an average of 1.32 mm, a standard deviation of 0.65 mm, a bias of 0.05 and a RMSE of 0.19 mm (Table 1). It is observed that the paired lengths have a very high correlation and that, in addition, the adjusted linear regression model is close to the y = x line (Fig. 7B). The elliptical confidence region (Equation (5)) includes the point $\beta_0 = 0$ and $\beta_1 = 1$ (Fig. 9). Thus, there are no significant differences between GT and nDGT regarding lengths.

Regarding diameters, it is observed that the average of the absolute errors ranges from 1.68 mm, for DGT, to 0.38 mm, for rDGT, and to 0.29 mm, for nDGT (Table 1). The same pattern is followed by the standard error, median, and standard deviation. In the same sense, it is observed that the elliptical confidence region is far from the point $\beta_0 = 0$ and $\beta_1 = 1$ for the DGT, and it is closer for the rDGT (Fig. 9A). nDGT is very close to being within the confidence region, in fact, it includes $\beta_0 = 0$ is very close to including $\beta_1 = 1$.

Analyzing length results, it is observed that DGT and nDGT faithfully

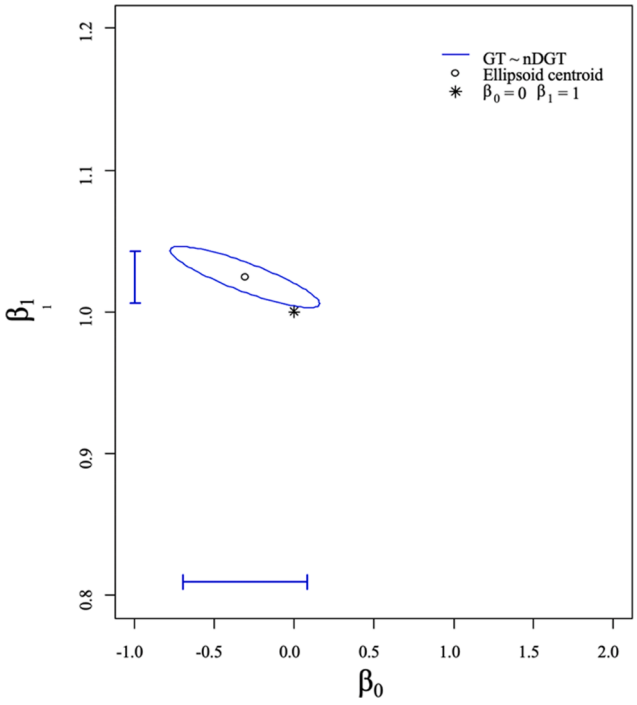

Fig. 6. Graphical representation of the elliptical confidence region described in Equation (5) for the ground-truth (GT) and the new digital ground-truth (nDGT) diameters comparison. The lines parallel to the axes represent the confidence intervals for each paramete with a 5 % significance level.

represent reality. The mean absolute error is 1.35 mm for DGT and 1.31 mm for nDGT, with a standard deviation of 1.94 mm and 1.60 mm, respectively (Table 1). The rDGT has an average absolute error of 9.10 mm and a standard deviation of 3.96 mm, which indicates that, by

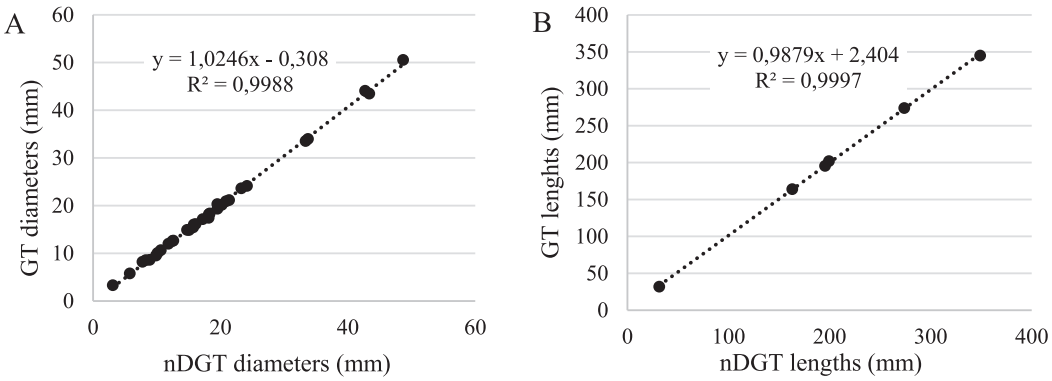

Fig. 7. Linear models adjusted between ground-truth (GT) and new digital ground-truth (nDGT) diameters (A) and lengths (B) including the line fit equation and the coefficient of determination.

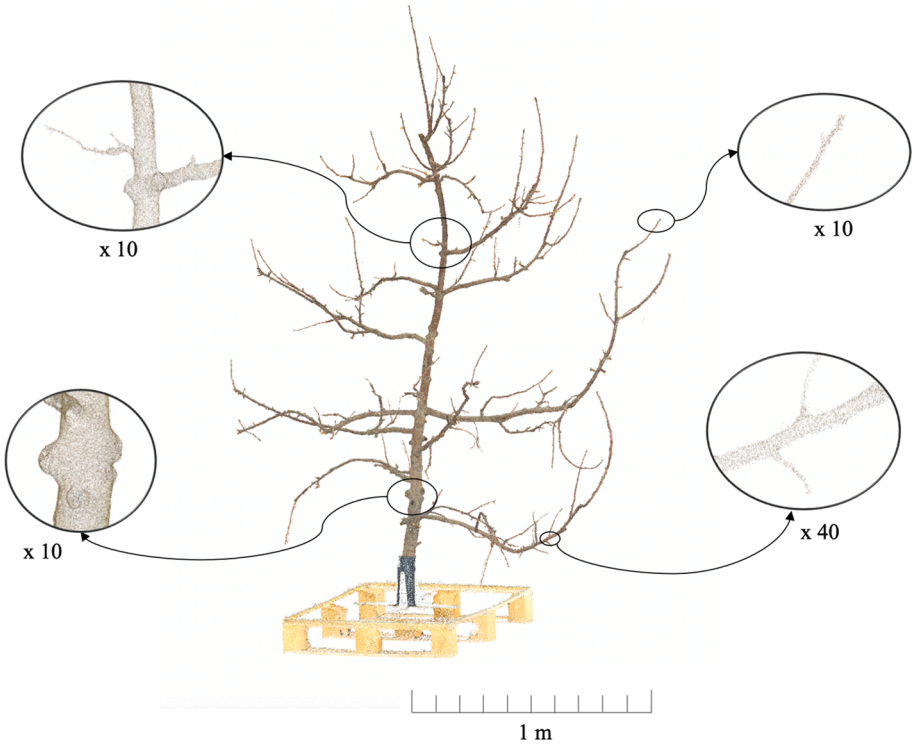

Fig. 8. nDGT point cloud with extended details at different zoom levels.

contracting the DGT to correct dehydration, the error of the diameters decreased but that of lengths increased. This is because the tree shrinks radially to the trunk or branch axes but practically not longitudinally when dehydrated (Stamm, 1935), while DGT was contracted in all three dimensions (x,y,z) towards the center of the point cloud. The lengths confidence region of the rDGT does not include the point $\beta_0 = 0$ and $\beta_1 = 1$ (Fig. 9B). In contrast, the point $\beta_0 = 0$ and $\beta_1 = 1$ was included within the confidence region of the DGT, before performing the contraction. Finally, the point $\beta_0 = 0$ and $\beta_1 = 1$, is also included within the nDGT confidence region regarding length.

Thus, it is observed that nDGT has an average error of 0.29 mm in diameters and 1.31 mm in lengths, a bias of − 0.15 mm in diameters and 0.05 mm in lengths and a RMSE of 0.49 mm in diameters and 1.97 mm in lengths (Table 1). The constructed model (nDGT) does not present statistically significant differences in lengths, but it does present significant differences in diameters (Fig. 9). Liu et al. (2018) measured diameters at breast height (DBH) using continuous photogrammetry in a forest environment and Miller et al. (2015) modeled 3D point clouds of individual trees using SfM and MVS photogrammetric techniques and tested the accuracy of height, diameter and volume estimates. Comparing the obtained diameters RMSE with Miller et al. (2015) and Liu et al. (2018), 9.2 mm and 2.14 mm, respectively, it is observed that the methodology proposed in this paper achieves much more accurate results.

4. Conclusions

A 3D point cloud (nDGT) was created using photogrammetry techniques (Structure from Motion and Multi-view Stereo) that faithfully represents reality. The bias of the model is −0.15 mm and 0.05 mm, for diameters and lengths, respectively. The developed methodology allows digital models to be created in field conditions with other sensing systems, compared to each other and validated with respect to a very accurate digital ground-truth, to be used with an actual tree ground-truth. The methodology used is time consuming, but it is useful as an extremely accurate digital ground-truth creation which can be used to validate

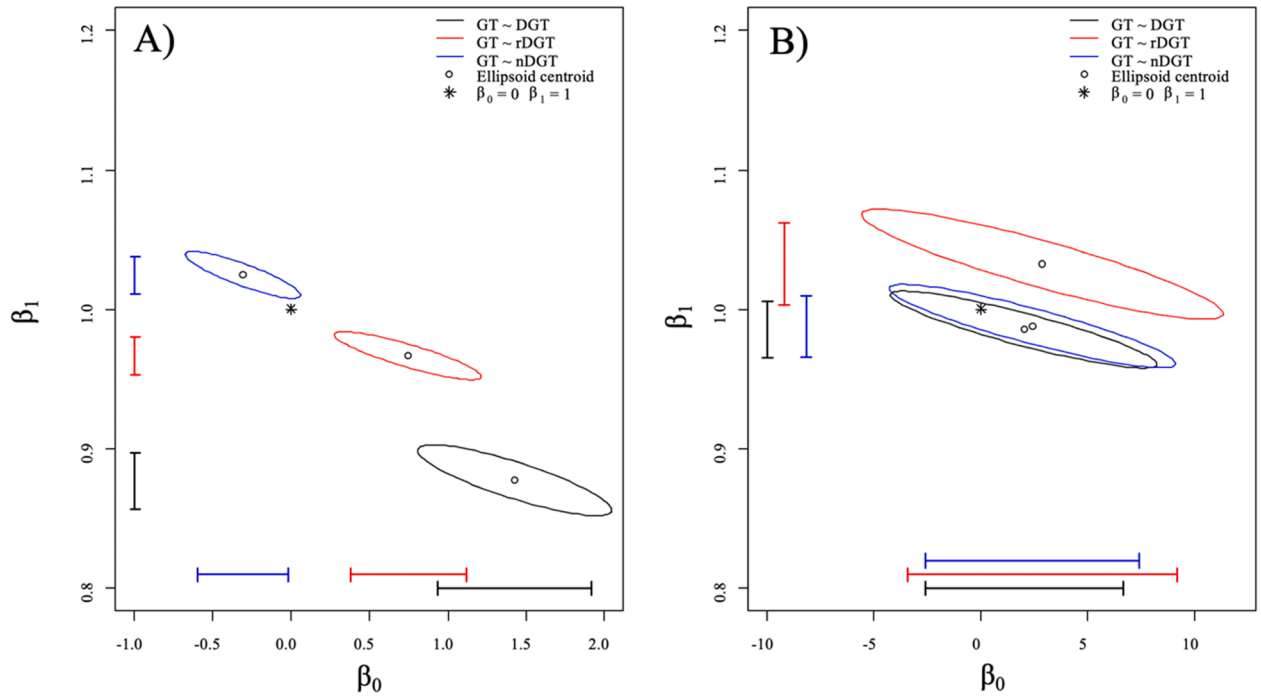

Fig. 9. Graphical representation of the elliptical confidence regions described in Equation (5) for each comparison (GT - DGT, GT - rDGT and GT - nDGT) for diameters (A) and lengths (B). The lines parallel to the axes represent the confidence intervals for each parameter with a 5 % significance level.

other sensing techniques.

Furthermore, the importance of dehydration has been collaterally detected. Most importantly, it has been shown that the proposed methodology can detect changes in trunk and branch diameters as well as in branch deformations caused by dehydration. Small diameter contractions can cause significant displacements in branches and the proposed methodology allows both of them to be quantified. This methodology may be useful in future studies in forestry and agronomy.

CRediT authorship contribution statement

Bernat Lavaquiol: Conceptualization, Methodology, Software, Validation, Formal analysis, Investigation, Resources, Data curation, Writing – original draft, Writing – review & editing, Visualization. **Ricardo Sanz:** Conceptualization, Methodology, Software, Formal analysis, Investigation, Writing – review & editing, Supervision. **Jordi Llorens:** Formal analysis, Data curation, Writing – review & editing, Visualization. **Jaume Arnó:** Data curation, Writing – review & editing, Visualization. **Alexandre Escolà:** Conceptualization, Methodology, Software, Formal analysis, Investigation, Resources, Data curation, Writing – original draft, Writing – review & editing, Visualization, Supervision, Funding acquisition.

Declaration of Competing Interest

The authors declare that they have no known competing financial interests or personal relationships that could have appeared to influence the work reported in this paper.

Acknowledgements

This research was funded by the Spanish Ministry of Economy and Competitiveness and the Ministry of Science, Innovation and Universities through the program Plan Estatal I+D+i Orientada a los Retos de la Sociedad, Project PAgFRUIT RTI2018-094222-B-I00. In addition, this work was also supported by the Secretaria d'Universitats i Recerca del Departament d'Empresa i Coneixement de la Generalitat de Catalunya under Grant 2017-SGR-646 and under the research grant program BFC2020S - Programa Santander Predocs UdL 2020. We would also like to thank Jaume Badia from Nufri for providing the tree used in this article as ground truth.

References

Aguilar, M. a., Pozo, J. L., Aguilar, F. J., Sanchez-Hermosilla, J., Páez, F. C., & Negreirosb, J. (2007). 3D Surface Modelling of Tomato Plants Using Close-Range. *The International Archives of the Photogrammetry, Remote Sensing and Spatial Information Sciences.*, *XXXVII*(2008), 139–144.

An, N., Welch, S.M., Markelz, R.J.C., Baker, R.L., Palmer, C.M., Ta, J., Maloof, J.N., Weinig, C., 2017. Quantifying time-series of leaf morphology using 2D and 3D photogrammetry methods for high-throughput plant phenotyping. Comput. Electron. Agric. 135, 222–232. https://doi.org/10.1016/j.compag.2017.02.001.

Arnó, J., Escolà, A., Vallès, J.M., Llorens, J., Sanz, R., Masip, J., Palacín, J., Rosell-Polo, J. R., 2013. Leaf area index estimation in vineyards using a ground-based LiDAR scanner. Precis. Agric. 14 (3), 290–306. https://doi.org/10.1007/s11119-012-9295-0.

EDF R&D Telecom ParisTech. (n.d.). *CloudCompare (version 2.6.1)*.

Escolà, A., Martínez-Casasnovas, J.A., Rufat, J., Arnó, J., Arbonés, A., Sebé, F., Pascual, M., Gregorio, E., Rosell-Polo, J.R., 2017. Mobile terrestrial laser scanner applications in precision fruticulture/horticulture and tools to extract information from canopy point clouds. Precis. Agric. 18 (1), 111–132. https://doi.org/10.1007/s11119-016-9474-5.

Forlani, G., Roncella, R., Nardinocchi, C., 2015. Where is photogrammetry heading to? State of the art and trends. Rendiconti Lincei 26 (1), 85–96. https://doi.org/10.1007/s12210-015-0381-x.

Gené-Mola, J., Gregorio, E., Auat Cheein, F., Guevara, J., Llorens, J., Sanz-Cortiella, R., Escolà, A., & Rosell-Polo, J. R. (2020). Fruit detection, yield prediction and canopy geometric characterization using LiDAR with forced air flow. *Computers and Electronics in Agriculture*, *168*(November 2019), 105121. 10.1016/j.compag.2019.105121.

González-Jorge, H., Riveiro, B., Arias, P., Armesto, J., 2012. Photogrammetry and laser scanner technology applied to length measurements in car testing laboratories. Measurement: Journal of the International Measurement Confederation 45 (3), 354–363. https://doi.org/10.1016/j.measurement.2011.11.010.

Goodbody, T.R.H., White, J.C., Coops, N.C., LeBoeuf, A., 2021. Benchmarking acquisition parameters for digital aerial photogrammetric data for forest inventory applications: Impacts of image overlap and resolution. Remote Sens. Environ. 265 (August), 112677 https://doi.org/10.1016/j.rse.2021.112677.

Grüner, E., Astor, T., Wachendorf, M., 2019. Biomass prediction of heterogeneous temperate grasslands using an SFM approach based on UAV imaging. Agronomy 9 (2), 54. https://doi.org/10.3390/agronomy9020054.

Gutiérrez, A., & Plaza, F. (1967). *Características físico-mecánicas de las madera españolas* (Instituto Forestal de Investigaciones y Servicio de la Madera (ed.)). Instituto Forestal.

Gutiérrez Oliva, A., & Plaza Pulgar, F. (1967). *Características físico-mecánicas de las maderas españolas*.

H. Lee, K., & Ehsani, R. (2009). A Laser Scanner Based Measurement System for Quantification of Citrus Tree Geometric Characteristics. *Applied Engineering in Agriculture*, *25*(5), 777–788. 10.13031/2013.28846.

International Society for Precision Agriculture (ISPA). (n.d.). *Precision Ag Definition*.

Jin, H., Soatto, S., Yezzi, A.J., 2005. Multi-view stereo reconstruction of dense shape and complex appearance. Int. J. Comput. Vision 63 (3), 175–189. https://doi.org/10.1007/s11263-005-6876-7.

Koci, J., Jarihani, B., Leon, J.X., Sidle, R.C., Wilkinson, S.N., Bartley, R., 2017. Assessment of UAV and ground-based structure from motion with multi-view stereo photogrammetry in a gullied savanna catchment. ISPRS Int. J. Geo-Inf. 6 (11), 8–10. https://doi.org/10.3390/ijgi6110328.

Liang, X., Jaakkola, A., Wang, Y., Hyyppä, J., Honkavaara, E., Liu, J., Kaartinen, H., 2014. The use of a hand-held camera for individual tree 3D mapping in forest sample plots. Remote Sensing 6 (7), 6587–6603. https://doi.org/10.3390/rs6076587.

Liu, J., Feng, Z., Yang, L., Mannan, A., Khan, T., Zhao, Z., Cheng, Z., 2018. Extraction of sample plot parameters from 3D point cloud reconstruction based on combined RTK and CCD continuous photography. Remote Sensing 10 (8), 1299. https://doi.org/10.3390/rs10081299.

Méndez, V., Catalán, H., Rosell-Polo, J.R., Arnó, J., Sanz, R., 2013. LiDAR simulation in modelled orchards to optimise the use of terrestrial laser scanners and derived vegetative measures. Biosyst. Eng. 115 (1), 7–19. https://doi.org/10.1016/j.biosystemseng.2013.02.003.

Miller, J., Morgenroth, J., Gomez, C., 2015. 3D modelling of individual trees using a handheld camera: Accuracy of height, diameter and volume estimates. Urban For. Urban Greening 14 (4), 932–940. https://doi.org/10.1016/j.ufug.2015.09.001.

Moriondo, M., Leolini, L., Staglianò, N., Argenti, G., Trombi, G., Brilli, L., Dibari, C., Leolini, C., Bindi, M., 2016. Use of digital images to disclose canopy architecture in olive tree. Sci. Hortic. 209, 1–13. https://doi.org/10.1016/j.scienta.2016.05.021.

Palacin, J., Palleja, T., Tresanchez, M., Teixido, M., Sanz, R., Llorens, J., Arno, J., Rosell, J.R., 2008. Difficulties on tree volume measurement from a ground laser scanner. *Conference Record - IEEE Instrumentation and Measurement Technology Conference*, *M* 1997–2002. https://doi.org/10.1109/IMTC.2008.4547376.

Palleja, T., Tresanchez, M., Teixido, M., Sanz, R., Rosell, J.R., Palacin, J., 2010. Sensitivity of tree volume measurement to trajectory errors from a terrestrial LIDAR scanner. Agric. For. Meteorol. 150 (11), 1420–1427. https://doi.org/10.1016/j.agrformet.2010.07.005.

Paulus, S., 2019. Measuring crops in 3D: Using geometry for plant phenotyping. Plant Methods 15 (1), 1–13. https://doi.org/10.1186/s13007-019-0490-0.

Rosell-Polo, J.R., Cheeinx, F.A., Gregorio, E., Andújar, D., Puigdomènech, L., Masip, J., Escolà, A., 2015. Advances in Structured Light Sensors Applications in Precision Agriculture and Livestock Farming. Adv. Agron. 133, 71–112. https://doi.org/10.1016/bs.agron.2015.05.002.

Rosell, J.R., Sanz, R., 2012. A review of methods and applications of the geometric characterization of tree crops in agricultural activities. Comput. Electron. Agric. 81, 124–141. https://doi.org/10.1016/j.compag.2011.09.007.

Sanz-Cortiella, R., Llorens-Calveras, J., Escolà, A., Arnó-Satorra, J., Ribes-Dasi, M., Masip-Vilalta, J., Camp, F., Gràcia-Aguilá, F., Solanelles-Batlle, F., Planas-Demartí, S., Pallejà-Cabré, T., Palacin-Roca, J., Gregorio-Lopez, E., Del-Moral-Martínez, I., Rosell-Polo, J.R., 2011. Innovative LIDAR 3D dynamic measurement system to estimate fruit-tree leaf area. Sensors 11 (6), 5769–5791. https://doi.org/10.3390/s110605769.

Stamm, A.J., 1935. SHRINKING and SWELLING of WOOD. Ind. Eng. Chem. 27 (4), 401–406. https://doi.org/10.1021/ie50304a011.

Talebpour, B., Türker, U., Yegül, U., 2015. The Role of Precision Agriculture in the Promotion of Food Security. Int. J. Agricul. Food Res. 4 (1), 1–23. https://doi.org/10.24102/ijafr.v4i1.472.

Walter, J., Edwards, J., McDonald, G., & Kuchel, H. (2018). Photogrammetry for the estimation of wheat biomass and harvest index. *Field Crops Research*, *216*(August 2017), 165–174. 10.1016/j.fcr.2017.11.024.

Westoby, M.J., Brasington, J., Glasser, N.F., Hambrey, M.J., Reynolds, J.M., 2012. "Structure-from-Motion" photogrammetry: A low-cost, effective tool for geoscience applications. Geomorphology 179, 300–314. https://doi.org/10.1016/j.geomorph.2012.08.021.

Yang, Q., Su, Y., Jin, S., Kelly, M., Hu, T., Ma, Q., Li, Y., Song, S., Zhang, J., Xu, G., Wei, J., Guo, Q., 2019. The influence of vegetation characteristics on individual tree segmentation methods with airborne LiDAR data. Remote Sensing 11 (23), 1–18. https://doi.org/10.3390/rs11232880.